# Study on Luminescence Mechanism of Nitrogendoped Carbon Quantum Dots and Application in Hg<sup>2+</sup> Detection

Lingyu Song<sup>1,2</sup>, Cheng Pu<sup>2</sup>, Lingling Ren<sup>2,a,\*</sup>, Jingji Zhang<sup>1,b,\*</sup>

<sup>1</sup>College of Materials and Chemistry, China Jiliang University, Hangzhou, Zhejiang, China <sup>2</sup>Technology Innovation Center of Graphene Metrology and Standardization for State Market Regulation, National Institute of Metrology (NIM), Beijing, China <sup>a</sup>renll@nim.ac.cn, <sup>b</sup>apzjj@cjlu.edu.cn \*Corresponding author

**Abstract:** Carbon quantum dots (CQDs) demonstrate significant capability for detecting heavy metal ions owing to their affordability, excellent water solubility, and photostability. Additionally, doping of CQDs with nitrogen atoms can introduce excellent electronic, chemical, and optical properties. Therefore, we used CA and EDA as precursors to prepare nitrogen-doped carbon quantum dots (N-CQDs) via a one-step hydrothermal process. They display a maximum emission peak at 443 nm with a quantum yield of fluorescence of 66.7%. The experiment clarified the formation process and described their fluorophore structures. Additionally, the N-CQDs demonstrate outstanding selectivity and sensitivity towards mercury ions ( $Hg^{2+}$ ). Consequently, a fluorescent detection method for  $Hg^{2+}$  was developed, which exhibits a broad linear detection range of 0 - 100  $\mu$ mol·L<sup>-1</sup> with a low limit of detection of 4 nM. Furthermore, the fluorescence quenching mechanism was further elucidated, and the potential utilization of this method for detecting  $Hg^{2+}$  in tap water samples was also confirmed.

Keywords: N-CQDs; mercury ions; fluorescent probe

#### 1. Introduction

The evolution of industrialization and urbanization has brought numerous achievements. However, escalating water pollution has emerged as a pressing environmental concern. Among the various pollutants in water bodies, heavy metal ion pollution is particularly prevalent. Due to their high relative density and large atomic mass, heavy metal ions are difficult to naturally degrade or eliminate. Among many heavy metal ions, although ions like Fe³+, Cu²+, Zn²+, and Mn²+ have lower toxicity, they can still impact the environment when present in high concentrations. On the other hand, Mercury ions (Hg²+) are among the most hazardous heavy metal ions. They have the potential to accumulate through the food chain, affecting human health, disrupting aquatic ecological balance, and impacting the growth of flora and fauna [1]. Therefore, developing highly sensitive and selective methods for detecting Hg²+ is crucial for monitoring environmental pollution, protecting public health, and maintaining ecological balance. Regarding Hg²+ detection technologies, traditional methods such as high-performance liquid chromatography (HPLC), generally rely on laboratory-grade analytical equipment. Not only are the maintenance costs of such instruments high, but the sample pretreatment processes are also complex and time-consuming, making them unsuitable for rapid on-site detection needs.

Carbon quantum dots (CQDs) were accidentally discovered by Xu et al. in 2004 over the course of carbon nanotube separation and purification [2]. In 2006, Sun et al. officially named them "carbon quantum dots," marking the formal inception of CQDs research [3]. Since then, researchers have conducted in-depth investigations into the synthesis strategies, physicochemical properties, and potential applications of CQDs. Although the luminescence mechanism of CQDs remains to be further clarified, many of their properties have already demonstrated significant application potential. Additionally, the fluorescent properties of CQDs can be modulated in various ways, such as by doping with heteroatoms such as nitrogen and sulfur, introducing different functional groups on the surface, or controlling their size distribution. These approaches not only enrich the functionalization strategies of CQDs but also significantly expand their applications. Due to their excellent photostability, high biocompatibility, and tunable fluorescence characteristics, CQDs serve as fluorescent probes that can rapidly provide detection results and significantly reduce monitoring costs, showcasing tremendous

potential in detecting heavy metal ion pollution.

In this paper, N-CQDs were prepared via a one-step hydrothermal process. They achieved a fluorescence quantum yield of 66.7% and exhibited good water solubility and solvent environment adaptability. Additionally, the formation process, their primary fluorophore structures, and the fluorescence quenching mechanism for Hg<sup>2+</sup> were further hypothesized. The Hg<sup>2+</sup> fluorescent detection method based on N-CQDs demonstrated a broad linear detection range and a low limit of detection. Furthermore, its potential application for detecting Hg<sup>2+</sup> in tap water samples was also validated.

# 2. Experimental section

### 2.1. Materials

Ethylenediamine (EDA), mercury(II) nitrate monohydrate, potassium chloride, magnesium chloride, Citric acid(CA), copper chloride, cadmium chloride, chromium chloride, zinc chloride, lead chloride, aluminum chloride, calcium chloride, sodium chloride, cobalt chloride were purchased from Aladdin. Dimethyl sulfoxide (DMSO), polyvinyl alcohol (PVA), anhydrous ethanol, methanol, N, N-dimethylformamide (DMF), isopropanol, acetone, and toluene were obtained from Thermo Fisher. All reagents were analytical grade and utilized without additional purification. Water purified from a Milli-Q system was used throughout the entire experiment.

# 2.2. Synthesis of N-CQDs

The preparation process of N-CQDs is depicted in Figure 1. First, a certain amount of CA and EDA were added to 20 mL of water. After being transferred to a 50 mL polytetrafluoroethylene (PTFE) lined autoclave, the mixture was subsequently heated at  $180^{\circ}$ C for 8 hours to yield the unpurified solution. The solution was coarsely filtered with a 0.22  $\mu$ m filter membrane and then purified with a dialysis bag for a day to obtain the N-CQDs solution. At last, the solution was freeze-dried at -55°C for 2 days to acquire N-CQDs powder.

During the experiment, the fluorescence quantum yield (QY) of N-CQDs was used as a criterion to optimize the synthesis conditions by varying the reaction temperature and the mass ratio of precursors. The results indicated that the optimal conditions were using a 50 mL PTFE-lined autoclave, a carbon source to nitrogen source mass ratio of 1:2 for the precursors, and a reaction temperature of  $180^{\circ}$ C while keeping the solvent volume and other conditions consistent. These findings are shown in Figure 2(a) and 2(b).

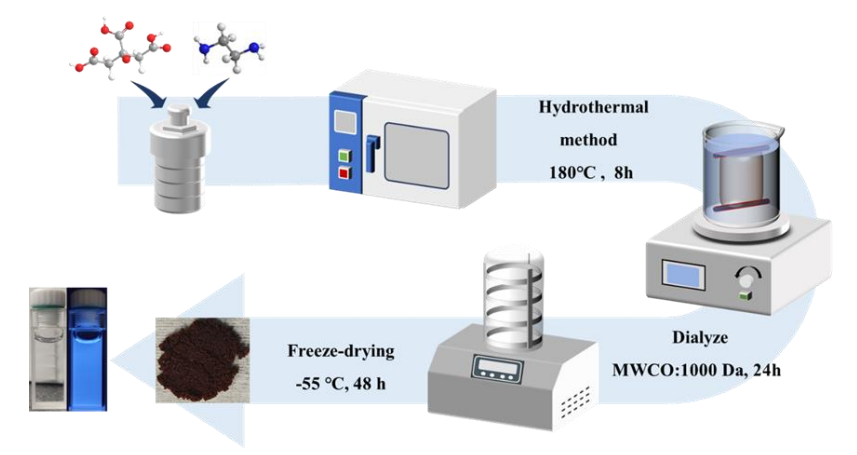


Figure 1: The preparation process of N-CQDs

### 2.3. Characterization

The microstructure of N-CQDs was characterized with a transmission electron microscope (TEM, G2 F20 U-TWIN, Tecnai) and an atomic force microscope (AFM, Multimode 8, Bruker). The chemical structure was determined by Fourier-transform infrared spectroscopy (FT-IR, Vertex 70, Bruker), and X-ray photoelectron spectroscopy (XPS, EscaLab 250Xi, Thermo Fisher Scientific). The fluorescence spectrum and absorption spectrum were characterized by a fluorescence spectrometer

(Nanolog-Kit FL3-2iHR, HORIBA) and a spectrophotometer (U-3900, Hitachi).

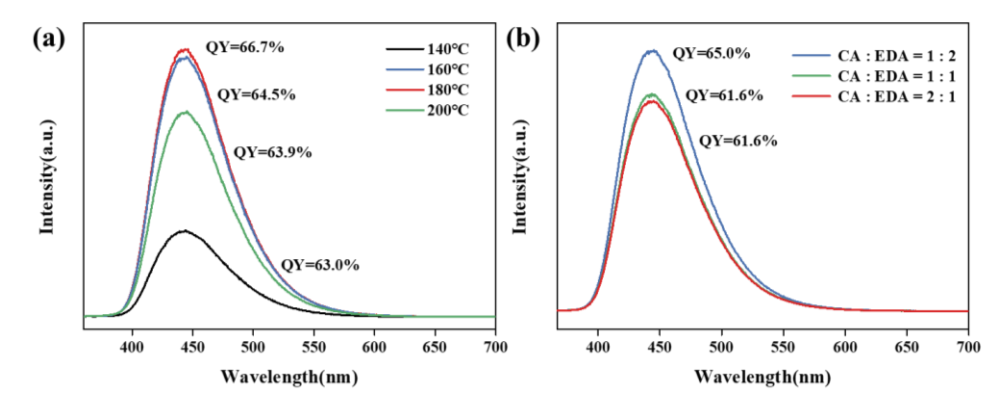


Figure 2: (a) fluorescence emission spectra and QY values at different reaction temperatures; (b) fluorescence emission spectra and QY values at 180°C with different precursor mass ratios

### 2.4. Measurement method of quantum yield

In this paper, the fluorescence quantum yield was measured by the absolute method, with the fluorescence spectrometer calibrated and traceable as described in reference [4].

# 2.5. Fluorescence sensing of Hg<sup>2+</sup>

N-CQDs were diluted with water, and solutions of  $K^+$ ,  $Mg^{2+}$ ,  $Na^+$ ,  $Zn^{2+}$ ,  $Cd^{2+}$ ,  $Cu^{2+}$ ,  $Ca^{2+}$ ,  $Ca^{2+}$ ,  $Pb^{2+}$ ,  $Al^{3+}$ , and  $Cr^{3+}$  were added to the N-CQDs solution to achieve a metal cation concentration of 10 mmol· $L^{-1}$  in the mixed system. The fluorescence emission spectra of the mixtures with various metal ions and N-CQDs were measured under 347 nm excitation light to assess the selectivity of N-CQDs for  $Hg^{2+}$ .

Additionally,  $100 \,\mu\text{L}$  of various concentrations of  $Hg^{2+}$  solutions were added to  $400 \,\mu\text{L}$  of N-CQDs solution, followed by water to bring the volume of the detection system to 3 mL. The fluorescence intensity at the emission wavelength of 443 nm was measured for different concentrations of  $Hg^{2+}$  solutions using an excitation wavelength of 347 nm. Each set of measurements was repeated three times, and the mean value was recorded.

# 2.6. Detection of $Hg^{2+}$ in tap water samples

The tap water samples were purified through a filter membrane to eliminate insoluble particulate impurities. Various concentrations of Hg<sup>2+</sup> solutions were added to 100 mL of the purified samples. The Hg<sup>2+</sup> content in the real water samples was measured using a fluorescence spectrometer.

# 3. Results and discussion

Firstly, the microstructure of N-CQDs was characterized by AFM and TEM. As depicted in Figure 3(a), it can be found that the N-CQDs synthesized via a hydrothermal process exhibited a well-defined elliptical morphology and good dispersion. Additionally, to precisely quantify the size distribution of these nanoparticles, particle size statistical analysis was performed on approximately 100 randomly selected nanoparticles, resulting in an average particle size of 4.78 nm for N-CQDs. Furthermore, AFM was employed to study the thickness dimensions of N-CQDs. From Figure 3(b), the average thickness ranges from 1 nm to 10 nm.

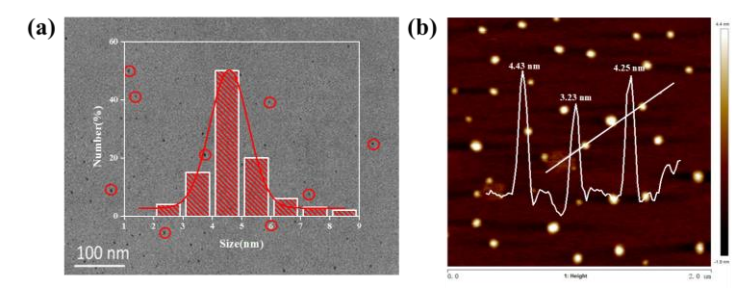


Figure 3: (a) TEM image with particle size distribution graph; (b) AFM image and thickness distribution graph of N-CQDs

For further investigation into the fluorescence mechanism, the properties of N-CQDs were characterized by FT-IR and XPS. As depicted in Figure 4, the wide absorption band at 3327 cm<sup>-1</sup> corresponds to the stretching vibrations of O-H and N-H groups. The characteristic absorption peak at 1651 cm<sup>-1</sup> indicates the presence of a C=O bond, and the peak at 1381 cm<sup>-1</sup> corresponds to the vibration of the C-N bond, indicating the formation of amide groups [5].

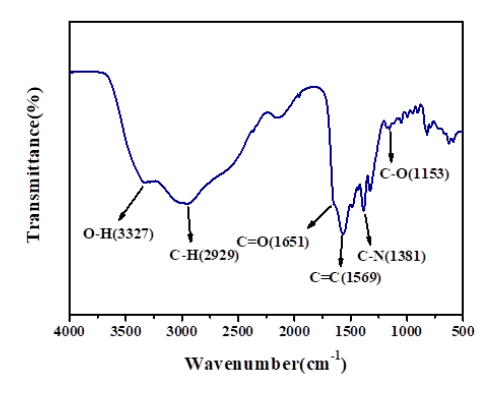


Figure 4: FT-IR spectra of N-CQDs

Subsequently, the elemental composition of N-GQDs was characterized by XPS spectroscopy. From Figure 5(a), three typical peaks are observed around 286.4 eV, 399.2 eV, and 532.1 eV, indicating that the primary composition of N-GQDs includes carbon, nitrogen, and oxygen elements. As depicted in Figure 5(c), the high-resolution N 1s spectrum reveals two important binding energy peaks at 399.53 eV and 401.28 eV, corresponding to pyridinic nitrogen and pyrrolic nitrogen. Additionally, the O 1s spectrum in Figure 5(d) further confirms the presence of C=O and C-O bonds. These results align with the conclusion from the FT-IR analysis, validating the successful nitrogen doping and the presence of hydrophilic functional groups on the surface of N-CQDs [6].

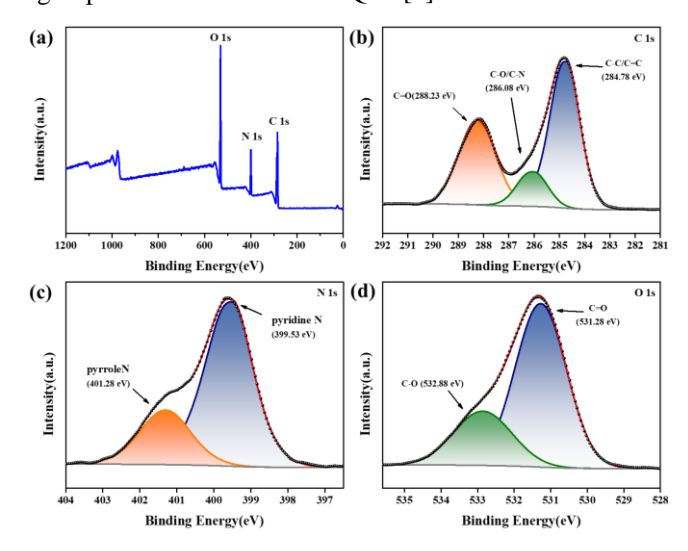


Figure 5: (a) XPS survey spectra; (b) C 1s spectra; (c) N 1s spectra; (d) O 1s spectra of N-CQDs

The absorbance of N-CQDs was characterized by a UV-visible spectrophotometer. As depicted in Figure 6(a), the absorption spectrum exhibits distinct absorption peaks at 219 nm and 297 nm. The prominent absorption peak at 219 nm primarily arises from the  $\pi \rightarrow \pi^*$  electronic transition of the C-C bonds within the conjugated structure of N-CQDs, indicating the presence of abundant conjugated systems in N-CQDs. The absorption peak at 297 nm arises from the  $n \rightarrow \pi^*$  electronic transition of unsaturated bonds such as C=C and C-N. This transition feature also introduces more defect states on their surface [7], leading to a change in the fluorescence emission wavelength.

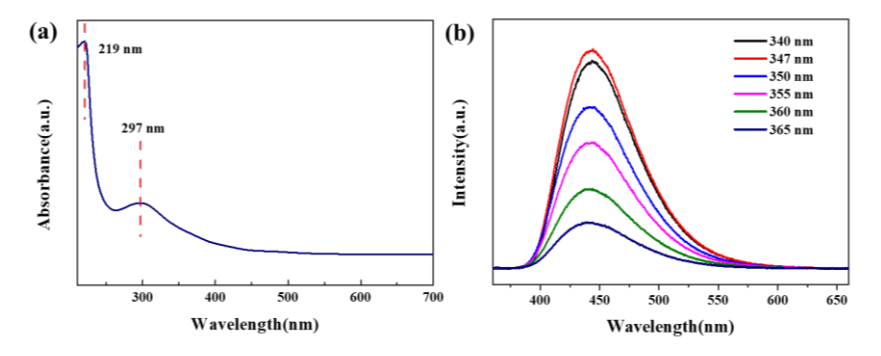


Figure 6: (a) UV-vis absorption spectrum; (b) fluorescence emission spectra of N-CQDs with varying excitation wavelengths

Subsequently, the fluorescence properties of N-CQDs were characterized by a fluorescence spectrometer. It was found that under light excitation at 347 nm, the quantum yield could reach 66.7%. As displayed in Figure 6(b), the emission peak position remains unchanged with varying excitation wavelengths across a range of different excitation wavelengths. This phenomenon reflects the wavelength-independent fluorescence characteristics of N-CQDs, which are attributed to the uniform distribution of sp<sup>2</sup>-hybridized carbon clusters as fluorescence emission centers and the stability of their surface states [8]. Combining the XPS and FT-IR characterization results, the formation mechanism of N-CQDs during synthesis and the primary fluorescent groups are speculated, as illustrated in Figure 7.

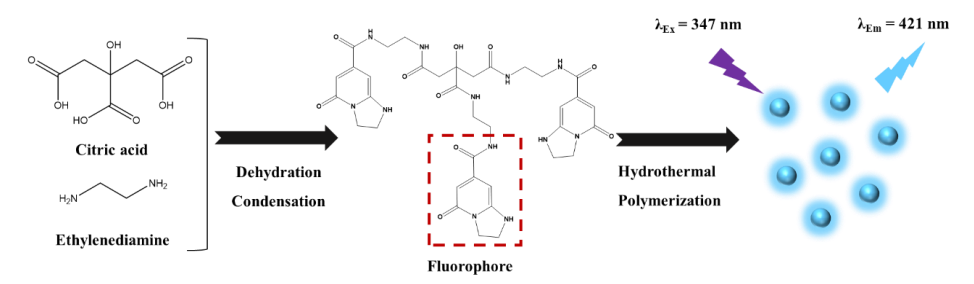


Figure 7: Formation mechanism of N-CQDs

Additionally, the application of N-CQDs in fluorescent films was explored, as shown in Figure 8. By mixing N-CQDs with polyvinyl alcohol (PVA) in a certain ratio and stirring the mixture evenly, a composite fluorescent film was successfully prepared by drop-casting onto a clean petri dish and drying. Under 365 nm UV light, these films emitted bright blue fluorescence.

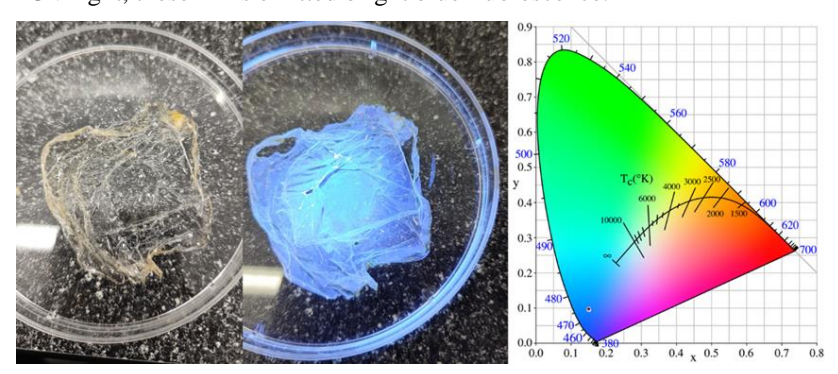


Figure 8: Application of N-CQDs/PVA composite fluorescence film and corresponding color coordinates

Selectivity in Hg<sup>2+</sup> sensing is crucial for the practical application of fluorescent detection methods. Therefore, multiple experiments were undertaken to assess the selectivity of N-CQDs solutions for detecting Hg<sup>2+</sup>. The results are depicted in Figure 9(a). The fluorescence intensity of solutions exhibited varying degrees of change when different types of metal ions were present.

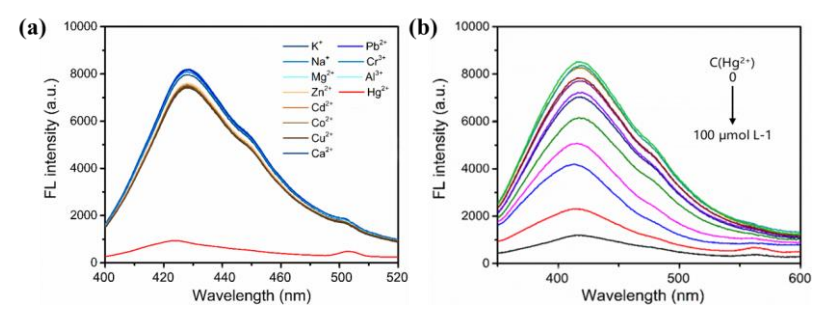


Figure 9: (a) Changes in fluorescence with the addition of various metal ions; (b) fluorescence emission spectra of N-CODs solution during titration with various concentrations of Hg<sup>2+</sup>

Furthermore, the sensitivity of N-CQDs to  $Hg^{2+}$  detection was investigated by performing fluorescence titration experiments with various concentrations of  $Hg^{2+}$  solutions. The fluorescence emission intensity at 443 nm was measured under 347 nm excitation, as shown in Figure 9(b), indicating that N-CQDs exhibit good sensitivity to  $Hg^{2+}$  detection.

To delve deeper into the detection mechanism, FT-IR and absorption spectra of N-CQDs were recorded with and without Hg<sup>2+</sup>. As depicted in Figure 10(a), the intensity of the nitrogen peak on the pyridine ring at 784 cm<sup>-1</sup> and the NH<sub>2</sub> peak on the alkyl group at 914 cm<sup>-1</sup> decreased. Simultaneously, the intensity of the peaks in the range of 2200-3400 cm<sup>-1</sup> increased, possibly indicating the formation of quaternary ammonium salts, secondary ammonium salts, and primary ammonium salts. This suggests that the chelation of N-CQDs with Hg<sup>2+</sup> primarily involves the amine groups.

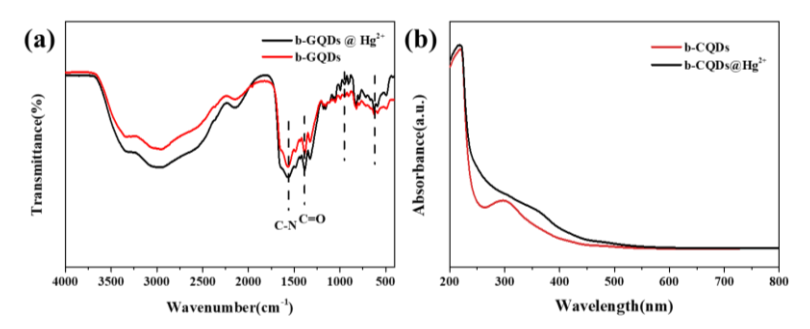


Figure 10: (a) FT-IR spectra and (b) UV-Vis absorption spectra N-CQDs, and N-CQDs@Hg<sup>2+</sup>

Subsequently, UV-visible absorption spectra were also measured. As depicted in Figure 10(b), upon the addition of a 100  $\mu$ mol·L<sup>-1</sup> Hg<sup>2+</sup> solution to the N-CQDs solution, the absorption peak at 297 nm broadened. This suggests that Hg<sup>2+</sup> binds to the nitrogen-rich regions of the N-CQDs. The speculation is that the nitrogen in the pyridine and pyrrole rings has lone pair electrons, which can chelate with Hg<sup>2+</sup>, inhibiting the emission of surface states in N-CQDs, and thereby causing fluorescence quenching phenomenon [9]. The schematic diagram of the mechanism is illustrated in Figure 11.

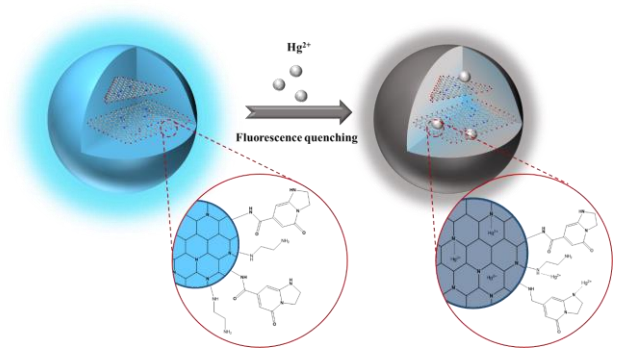


Figure 11: Fluorescence detection mechanism of N-CQDs@Hg<sup>2+</sup>

Based on the change in relative fluorescence intensity, we plotted the standard curve, as shown in Figure 12. When the added  $Hg^{2+}$  falls within the range from 0 to 100  $\mu$ mol·L<sup>-1</sup>, a strong linear correlation exists between the fluorescence intensity of N-CQDs and the concentration of  $Hg^{2+}$ , characterized by a linear equation of y = 0.2265 + 0.8861x ( $R^2 = 0.998$ ), where y represents the relative fluorescence intensity and x signifies the concentration of  $Hg^{2+}$ . According to the IUPAC standard ( $3\sigma/k$ ), the calculated detection limit of this detection method is 4 nmol·L<sup>-1</sup>.

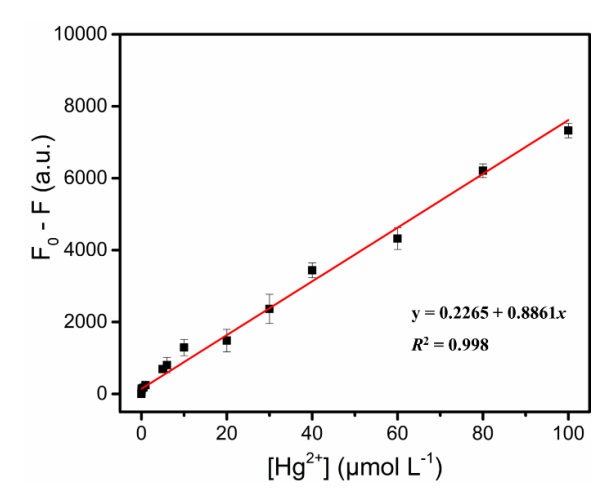


Figure 12: Curve showing the relative fluorescence intensity signal as a function of  $Hg^{2+}$  concentration Table 1: Detecting  $Hg^{2+}$  Content in Tap Water Samples Based on N-GQDs

Sample	Additive Content (mol·L <sup>-1</sup> )	Detected Content (mol·L <sup>-1</sup> )	Recovery (%)	RSD (%)
1	20.00	20.12±0.18	106.0±9.0	6.58
	50.00	50.45±0.13	109.0±2.6	1.71
	100.00	100.85±0.17	108.5±1.7	0.11
2	20.00	20.47±0.04	123.5±2.0	1.32
	50.00	50.61±0.03	112.2±0.6	0.22
	100.00	110.12±0.03	111.2±0.3	2.21

The concentration of Hg<sup>2+</sup> in actual tap water samples was measured, and the precision and dependability of this detection method were verified through spike recovery experiments. Upon laboratory conditions, two groups of samples were tested by the fluorescence method. After adding known concentrations of Hg<sup>2+</sup>, the recovery rates ranged from 106.0% to 123.5%, as illustrated in Table 1. This range of recovery rates indicates that the fluorescence detection method utilizing N-CQDs is not only capable of effectively detecting Hg<sup>2+</sup> in actual samples but also demonstrates excellent accuracy.

### 4. Conclusion

In this paper, N-CQDs were prepared via a one-step hydrothermal process. The high fluorescence quantum efficiency is primarily attributed to the amide condensation reaction between CA and EDA during the synthesis process, which allows nitrogen atoms to be doped into the carbon structure. This process not only facilitates the formation of numerous sp²-conjugated fluorescence emission centers (such as pyridinic nitrogen) but also creates stable defect states on the surface. These characteristics enhance the outstanding optical performance of the N-CQDs.

Additionally, a fluorescence detection method for  $Hg^{2+}$  based on N-CQDs was developed. With the optimal detection conditions determined in the experiment, this method showed a wide linear detection range from 0 to 100  $\mu$ mol·L<sup>-1</sup> and achieved a low detection limit of 4 nmol·L<sup>-1</sup>. These performance metrics reveal the potential of N-CQDs as a highly effective fluorescent probe for detecting  $Hg^{2+}$  in water.

### References

[1] Mukherjee S, Bhattacharyya S, Ghosh K, et al. Sensory development for heavy metal detection: A

### Academic Journal of Materials & Chemistry

### ISSN 2616-5880 Vol. 5, Issue 3: 9-16, DOI: 10.25236/AJMC.2024.050302

- review on translation from conventional analysis to field-portable sensor[J]. Trends in Food Science & Technology, 2021, 109: 674-689.
- [2] Xu X, Ray R, Gu Y, et al. Electrophoretic Analysis and Purification of Fluorescent Single-Walled Carbon Nanotube Fragments[J]. Journal of the American Chemical Society, 2004, 126(40): 12736-12737.
- [3] Sun Y P, Zhou B, Lin Y, et al. Quantum-Sized Carbon Dots for Bright and Colorful Photoluminescence [J]. Journal of the American Chemical Society, 2006, 128(24): 7756-7757.
- [4] Zhili J, Cheng P, Lingling R. Study on Absolute Measurement Method of Fluorescence Quantum Efficiency[Z]. Metrology Science and Technology: 66. 2022: 17.
- [5] Li H, Zhang Q, Luo X, et al. Intrinsic dual emissive carbon dots for ratiometric sensing of acetylcholinesterase fluctuation induced by organophosphorus pesticide intoxication[J]. Sensors and Actuators B: Chemical, 2022, 373: 132590.
- [6] Zhao H, Liu G, You S, et al. Gram-scale synthesis of carbon quantum dots with a large Stokes shift for the fabrication of eco-friendly and high-efficiency luminescent solar concentrators[J]. Energy & Environmental Science, 2021, 14(1): 396-406.
- [7] Dang T H T, Mai V T, Le Q T, et al. Post-decorated surface fluorophores enhance the photoluminescence of carbon quantum dots[J]. Chemical Physics, 2019, 527: 110503.
- [8] Zhu S, Meng Q, Wang L, et al. Highly Photoluminescent Carbon Dots for Multicolor Patterning, Sensors, and Bioimaging[J]. Angewandte Chemie International Edition, 2013, 52(14): 3953-3957.
- [9] Mintz K, Waidely E, Zhou Y, et al. Carbon dots and gold nanoparticles based immunoassay for detection of alpha-L-fucosidase[J]. Analytica Chimica Acta, 2018, 1041: 114-121.